Depletion of intermediate filament IFB-1 negatively affects mobility and physiological function of mitochondria in *C. elegans* sensory neurons

Yen Chang[‡], Muniesh Muthaiyan Shanmugam[‡], Prerana Bhan, Syed Nooruzuha Barmaver, Gong-Her Wu and Oliver I. Wagner*

National Tsing Hua University, Institute of Molecular and Cellular Biology, Department of Life Science, 30013 Hsinchu, Taiwan (R.O.C.)

[‡]Both authors contributed equally to this study.

Short title: IFB-1 affects mitochondrial motility

***Corresponding author**:

Dr. Oliver I. Wagner

Professor

National Tsing Hua University

Institute of Molecular and Cellular Biology & Department of Life Science

101, Sec. 2, Kuang Fu Road, Hsinchu 30013, Taiwan (R. O. C.)

Email: owagner@life.nthu.edu.tw

Phone: +886-3-574-2487

Fax: +886-3-571-5934

ABSTRACT

Mitochondria and intermediate filaments (IF) accumulations often occur during imbalanced axonal transport leading to various types of neurodegenerative diseases. It is still poorly understood whether a link between neuronal IFs and mitochondrial mobility exist. In *C. elegans*, among the 11 cytoplasmic IF family proteins, IFB-1 is of particular interest as it is expressed in a subset of sensory neurons and forms an obligate heteropolymer with one of the essential IFA proteins critical for worm viability. Depletion of IFB-1 leads to dye-filling and chemotaxis defects as well as reduced life span. Axons grew shorter during development and mitochondria transport is slowed down leading to reduced densities of these organelles in neurons. Oxygen consumption and mitochondrial membrane potential is measurably reduced in worms carrying mutations in the ifb-1 gene. Membrane potential also seemed to play a role in transport such as after FCCP treatment increased directional switching of mitochondria are observed. Mitochondria colocalize with IFB-1 in worm neurons and appear in a complex with IFB-1 in pull-down assays. In summary, we propose a model in which neuronal intermediate filaments may serve as transient anchor points for mitochondria during their microtubule-based long-range transport in neurons.

Keywords: Axonal transport, mitochondria, intermediate filaments, *C. elegans*, amphid sensory neuron bundle, FCCP, ATP5B1, IFB-1, IFA, chemotaxis quadrant assay, nematode oxygen consumption

INTRODUCTION

The neuronal cytoskeleton is composed of three major cytoskeletal elements: actin, microtubules and intermediate filaments (IFs). IFs are divided into six classes based on their sequence homologies, and in mammalian neurons a diverse set of IFs can be found, including synemin, peripherin, vimentin, nestin, α-internexin and neurofilaments (NFs). Abnormal accumulations of NFs can be found in various neurological diseases such as Alzheimer's disease, Parkinson's disease and amyotrophic lateral sclerosis (ALS), while many of the aforementioned IFs (specifically peripherin and α-internexin) are known to be central components of neurofilaments [1-5].

In *C. elegans*, the IF family is composed of eleven IF proteins that can be divided into two categories based on their expression pattern: IFB-2, IFC-1, IFC-2, IFD-1, IFD-2, and IFP-1 belong to one category of IF proteins that localize to the intestinal terminal web where they provide mechanical flexibility to the intestinal lumen. The other category includes IFA-1, IFA-2 (previously named MUA-6), IFA-3, IFA-4 and IFB-1. In this category, IFB-1 co-expresses and forms obligate heteropolymers with either one of the IFAs. These IFs are widely expressed in worms and except IFA-4, all are essential for viability [6-8]. Among these IFs, IFA-1, IFA-2, and IFB-1 particularly attracted our attention as they are reported to be expressed in *C. elegans* amphid neurons [7]. Since IFB-1 forms heteropolymers with IFA-1 and IFA-2 [8], we focused on the essential IFB-1 and its presumed effects on mitochondrial transport in amphid sensory neuronal bundles. To monitor mitochondria in the amphid sensory neuron bundle and to overexpress IFB-1 for colocalization experiments we employed the *Posm-5* promoter known to drive the expression of genes in amphid, labial and phasmid sensory neurons [9, 10].

As a result of alternative splicing, IFB-1 can be found in two isoforms, IFB-1A and IFB-1B. IFB-1A and IFB-1B transcripts comprise different promoters and distinct first exons but share the remaining C-terminal domains (Figure 1N); therefore, IFB-1A and IFB-1B differ in their N-terminal head domains. Although two IFB-1 isoforms are slightly different in their expression sites and functions, they are both required for muscle attachment and epidermal elongation at the 2-fold stage in *C. elegans* embryonic development. Both IFB-1 isoforms localize to epidermal attachment structures linking muscles to cuticles. An antibody raised against the C-terminal region of IFB-1 does detect both isoforms of IFB-1, whereas in worms carrying the *ju71* mutant allele (which removes the promoter region of the *ifb-1* gene) only the isoform IFB-1B can be detected by Western blots [11]. Another allele *ok1317* exist but hasn't been characterized yet. Our analysis revealed that it carries a 1361 bp deletion in the promotor region, 1032 bp upstream of the start codon of *ifb-1a* (and both *ju71* and *ok1317* located in the first intron of *ifb-1b*) (Figure 1N). To monitor the effect of IFB-1A on mitochondria motility we employed both alleles.

Mitochondria produce ATP via the oxidative phosphorylation chain, whereas a toxic by product, ROS (reactive oxygen species), is known to damage cellular components and mtDNA. Mutations in mtDNA are accumulated over lifetime resulting in reduced mitochondrial function with aging. In many neurodegenerative diseases (with impaired axonal transport) mitochondria are selectively targeted for damage. For example, mutations in the mitochondrial proteins PINK1, mitofusin 2 and paraplegin are causatives of Parkinson's disease. HSP, CMT and mutant forms of SOD1, parkin, huntingtin, PARK1/DJ-1 all damage mitochondria. Amyloid-β-peptide, the neurotoxin MPP+ and excitotoxic glutamate damage mitochondria, and at the same time impair axonal transport; resulting in increased net retrograde movements of mitochondria with the

consequence that these organelles accumulate in somas. Axonal depletion of mitochondria and accumulations in somas can be seen in human ALS cases, therefore mitochondria are not only damaged in mutant SOD1 axons but also their number in axons is severely reduced [2, 4, 12].

The current understanding of mitochondrial transport is that conventional kinesin-1 (KIF5) and dynein are attached at the same time to a mitochondrion, occasionally pulling in opposite directions, thus causing bidirectional and saltatory movements of these organelles. Recently, adaptor proteins have been described to facilitate binding of KIF5 to mitochondria (syntabulin or miro/milton) revealing the complexity of motor-organelle recognition [3, 5, 13]. To keep mitochondria stationary (only about one third of axonal mitochondria are mobile), theories exist that interactions with actin (at the axonal cortex or in growth cones) [14] or NFs [15] may occur; and more recently, a protein SNPH (syntaphilin) was identified that directly docks (cross-links) mitochondria to microtubules [16]. The importance of immobilizing mitochondria on their move within neuronal (or non-neuronal) cells lies in their localized distribution depending on cellular ATP needs. Indeed, it was demonstrated that mitochondria accumulate at those areas where ATP (and calcium) consumption is high [17]. Based on the thin diameter of the axon and its crowded internal [18] it is apparent that large organelles such as mitochondria may reside in close proximity to cytoskeletal elements other than microtubules. These filamentous elements include actin and IFs that might act as static anchor-points to immobilize mitochondria [19]. Importantly, in non-neuronal cells, IF proteins (other than NFs) were reported to affect mitochondrial morphology, distribution and motility. For example, it has been shown that vimentin directly binds to mitochondria to affect mitochondrial morphology, organization and mobility in fibroblasts [20, 21]. Furthermore, it was revealed that the IF-associated protein plectin 1b is able to link mitochondria to the IF-network in fibroblasts [22].

This study demonstrates the importance of neuronal intermediate filaments in the mitochondrial trafficking and function along the long dendrites of amphid sensory neurons.

MATERIAL AND METHODS

Worm maintenance, strains and plasmids

Worms were maintained at 20°C on NGM agar plates seeded with OP50 *E. coli* according to standard methods [23] . Strains CZ4380 *ifb-1(ju71)* and RB1253 *ifb-1(ok1317)* were received from the CGC (Caenorhabditis Genetics Center, Minnesota, USA). The *ju71* allele carries a 617 bp deletion that removes the promoter region of *ifb-1a* (Figure 1N) abolishing the expression of IFB-1A (but not IFB-1B) protein based on Western blots [11, 24]. The *ok1317* has not been characterized yet and based on our analysis it carries a 1361 bp deletion located upstream of the *ju71* deletion, yet residing in the *ifb-1a* promoter region. Both alleles (*ju71* and *ok1317*) likely remove parts of promoter of ifb-1a gene likely effecting the expression level of the gene (Figure 1G+N). In order to visualize mitochondria in *C. elegans* amphid sensory neuron bundles, we chose to employ the *Posm-5* promoter known to selectively express genes in amphid, labial and phasmid neurons [9, 10]. Here we used an existing construct *Posm-5::xbx-1::yfp* [25] and replaced the *xbx-1::yfp* insert with an *mito::gfp* insert (encoding for a C-terminal GFP fused to an N-terminal mitochondria-targeting sequence) amplified from the Andrew Fire vector pPD96.32 (Plasmid #1504, Addgene, Cambridge, MA). The resulting plasmid *Posm-5::mito::gfp* was coinjected with the roller marker pRF4*(rol-6(su1006))* into N2 worms (at both 100 ng/µl) using standard microinjection techniques [26, 27]. *N2;nthEx4[Posm-5::mito::gfp;rol-6(su1006)]* worms were then crossed with the aforementioned strains CZ4380 and RB1253, respectively, and genotyped for homozygosity using following primers: For the *ju71* mutation 5'-CCGATTTATTGCAAGATGGTGTAGA-3' (forward), 5'- TCAATGGTTTTGCCTTCCCG-3'

(reverse) and for the *ok1317* mutation 5'-AATCAGCGCCACAGGC-3' (forward) and 5'-GCAACCAATTTACGGTTCTG-3'(reverse). For colocalization experiments, we constructed a *Posm-5::ifb-1a::mrfp* vector by subcloning the *ifb-1* insert from and existing vector pCZ454 *Pifb-1::ifb-1a::gfp* (a kind gift from Dr. Andrew Chisholm) and the *mrfp* from an existing vector *Punc-104::snb-1::mrfp* [28]. *Posm-5::ifb-1a::mrfp* was then coinjected with *Posm-5::mito::gfp* (at both 100 ng/µl) and pRF4*(rol-6(su1006))* (50 ng/µl) into N2 worms to obtain the strain *N2;nthEx5[Posm-5::ifb-1a::mrfp;Posm-5::mito::gfp;rol-6(su1006)]*. Complementary DNA of *ifb-1* was cloned into pEGFP-N3 (gift from Prof. Yin-Chang Liu) using AAAAGCTAGCATGGAGGCTGAATCAGC (forward) and AAAAGGTACCTTGTCCGGATTGGATGG (reverse) between NheI and KpnI restriction sites and used for transfection into SW13 (vim-) cells.

Dye-filling and chemotaxis quadrant assay

To investigate dye uptake of sensory neurons we incubated worms in M9 buffer containing a final concentration of 0.1 mg/ml DiI (1,1'-dioctadecyl-3,3,3'3'-tetramethylindo-carbocyanine perchlorate, Sigma Aldrich) in 0.5% Triton X-100 [29]. After 2 hours incubation on a rotator, worms were subsequently mounted on 2% agarose pads and anesthetized with 5 mM tetramisole (Sigma-Aldrich) for observation under a fluorescence microscope.

Standard quadrant assay to test chemotaxis of worms was performed as described by Margie et al. [30]. NGM plates (5 cm, without OP50) were prepared according to the protocol and 100 to 200 synchronized worms at the young adult stage were transferred to the center of each plate. Plates were inverted and incubated at room temperature for 1 to 2 hours. After incubation, worms at different quadrants were counted immediately. 2 µl of chemoattractant (0.5% diacetyl mixed with equal volume of 0.5 M sodium azide) and control solution (0.5 M

sodium azide mixed with equal volume of ddH_2O, the solvent for diacetyl) were placed at appropriate positions just before the addition of worms. Chemotaxis index is calculated by: CI = (number of worms in test quadrants)-(number of worms in control quadrants)/total number of worms.

Mitochondria motility, particle size and colocalization analysis

To record the movement of mitochondria in amphid sensory neuron bundles of living *C. elegans*, we immobilized the animals using 5 mM tetramisole (Sigma-Aldrich) before placing them on 2% agarose-coated objective slides. An Olympus IX81 microscope with a DSU Nipkow spinning disk unit connected to an Andor iXon DV897 EMCCD camera was employed for high-resolution and high-speed time-lapse imaging (3-4 frames per second). To create kymographs from recorded videos, we used the image processing and analysis software NIH ImageJ 1.47 (NIH, http://rsb.info.nih.gov/ij/). The software allows to draw a line over a neuron of interest (within the video) and by applying the so called "reslice stack" function, the result is a stack of single sequences from the movie at the defined area. Static particles then appear as vertical lines while moving particles leave traces on horizontal directions, whereas slopes of these traces correspond to the velocities of these particles (kymograph examples in Figure 2). Curved neurons were straightened before their conversion into kymographs using the "straighten curved objects tool" from Kocsis et al. [31]. A moving event is defined as a single motility occurrence typically right after a pause or a reversal and, vice versa, it ends when the particle is again pausing or reversing. Mitochondrial moving distances larger than 1.6 µm were classified as "processive", otherwise as "vibrating" (see also [32]). For mitochondria particle analysis such as area, Feret's diameter and density, we used the "particle analysis" plugin from ImageJ (Figure 3). For neurite length (Figure 1K+M), we used the "line measurement tool. For colocalization

analysis we used the "intensity correlation analysis" plugin from ImageJ according to a method developed by Li et al. [33] (Figure 5F+6F). The intensity correlation quotient (ICQ) (Figure 6F) is based on the PDM (product of the differences from the mean) that is equal to: (red intensity – mean red intensity) × (green intensity – mean green intensity). ICQ values range from -0.5 to 0.5 with values close to 0.5 standing for interdependent expression of two fluorophores, close to -0.5 for segregated expression and values near 0 for random expression of two fluorophores.

Note that a study reports mild changes of RAB-3 vesicle motility in *C. elegans* neurons when employing 10 mM levamisole [34] (about 0.05 µm/s faster in anterograde directions). Given that we used half of the reported concentration (5 mM tetramisole), we expect negligible effects. Most important, we used tetramisole for both the control (wild type) and experiment (mutants) (efficiencies of levamisole and tetramisole are comparable).

Of further note is that since the *Posm-5* promoter express in amphids, labials and tail phasmids [9, 10], we have to be able to distinguish these neurons from each other (as we wish to focus on amphids only for this study based on the reported expression pattern of IFB-1). To approach this concern, we only investigate worms that are placed with their vulva facing sidewise (and not up or downwards). In this position, amphids can be clearly distinguished from labials, as labials are facing more outwards (close to the worm's lateral cuticle) while amphids are running along the inner pharynx adopting it's shape. Also, in the confocal microscope amphids seem to be located in different focal planes than labials. All investigated worms in this study are young adult stage.

RT-qPCR

For RT-qPCR (reverse transcription quantitative PCR), we designed the following primers that cover the 1st and 3rd exon (229 bp) of the *ifb-1a* gene: 5'-AATCAGCGCCACAGGC-3' (forward) and 5'-CAACCAATTTACGGTTCTG (reverse). As an internal control we used the frequently employed *cdc-42* gene [35] with the following primer set: 5'-CTGCTGGACAGGAAGATTACG-3'(forward) and 5'-CTCGGACATTCTCGAATGAAG-3'(reverse). To quantify PCR products, we used the ABI Power SYBR Green PCR Master Mix (ABI, USA) in conjunction with an ABI 7500 real-time PCR machine.

Whole worm oxygen consumption analysis

Oxygen consumption analysis was performed according to a method described by Yamamoto et al. [36] employing the XF24 Extracellular Flux Analyzer (Seahorse Bioscience Inc., USA). Worms were synchronized to obtain young adults for analysis and washed several times before placing them on NGM agar plates without OP50. 50 worms were then picked to each vial of standard 24-well Seahorse plates (#100777-004) containing 200 µl of M9 buffer. Four of these 24-wells were used for background correction (only buffer) and all remaining wells were divided equally for two different experimental groups (N2 and *ifb-1(ok1317)* or N2 and *ifb-1(ju71)*). Oxygen consumption by the worms from the medium was measured 15 times over a period of 120 min. Data from different experimental groups were analyzed using Student's t-test.

Life span assay

The life span assay protocol described by [37] was slightly modified, where we age synchronized worms by timed egg laying on a plate for 2-3 hrs. Worms were then transferred to newly prepared NGM plates with heat-killed [38] (65ºC for 15 min) OP50 *E. coli* and transferred

to new plates every day. Dead worms were identified by their motionlessness when prodded with a platinum wire. Dead worms were then scored excluding those worms that disappeared or died by otherwise causes.

Worm neuronal culture

Neuronal cell isolation in *C. elegans* was performed based on the protocols by Christensen et al. [39] and Strange et al. [40] Isolated neurons are maintained in Leibowitz's (L15) medium topped with 10% fetal bovine serum (FBS), 100U/ml of penicillin, 100 µg/ml of neomycin and 100 µg/ml of streptomycin respectively. These neuronal cells can be stored at 20°C without the need of adjusting the CO2 atmosphere. The experiments were performed 4 times and images were taken at day-2.

Mammalian cell culture

Mammalian cell line SW13 (vim-) was a kind gift from Prof. Perng, Ming-Der (National Tsing Hua University, Taiwan). SW13 (vim-) cells were cultured in DMEM medium with 10% fetal bovine serum at 37°C with 5% CO_2 atmosphere. At 70-80% confluency, cells were transfected with the plasmid constructs pEGFP-N3 ifb-1 and pEGFP-N3 without any insert as control (empty vector) using K2® transfection system from Biontex (Germany) as per the kit instructions.

Mitochondrial pull down assay and Western blotting

SW13 cells were washed with PBS thrice to remove the culture media and trypsinized, followed by resuspension in isolation buffer and homogenized on ice using a glass homogenizer with 20 to 25 strokes. Homogenized solution was then centrifuged at 1000 g at 4°C for 10 min.

The supernatant was collected and centrifuged at 14,000 g for 15 min at 4°C gaining a cytosolic fraction and the pellet containing crude mitochondria. The pellet was then washed twice with isolation buffer and both cytosolic and mitochondrial fractions were quantified for its protein concentration using Thermo Scientific Pierce™ BCA protein assay kit (#23225), whereas 30 µg of protein was used for Western blotting analysis. 8% SDS-PAGE was used for protein separation by electrophoresis and transferred to a PVDF blot Immobilon®-P, Millipore Corporation (IPVH00010). 10% BSA was used to block the membrane followed by protein detection using a primary antibody of 1:1000 dilution (anti-β actin antibody (C4, SC-47778, mouse monoclonal antibody, Santa Cruz Biotechnology, USA) or anti-GFP antibody (B-2, SC-9996, mouse monoclonal, Santa Cruz Biotechnology, USA) or ATP5B1 antibody (Gene Tex Inc.)) as well as secondary antibody of 1:5000 dilution in conjunction with Luminata™ Classico Western HRP substrate (Millipore Corporation, (WBLUC0500)).

TMRE staining

TMRE staining of *C. elegans* was performed as described in [41] with little modification. Young adult worms were washed with M9 buffer to remove the bacteria. TMRE dye (TMRE dye is a kind gift from Prof. Chuang Rung Chang) with a final concentration of 300 nM in M9 was added and kept in rotation for 8 hours at 20°C in the dark. The worms were washed four times with M9 buffer and were put down on OP50 seeded NGM plates for 1-2 hours in the dark at 20°C. Worms were then mounted into 2% agarose pads for imaging.

RESULTS

Several reports demonstrate direct IF-mitochondria interactions and the effect of IFs on the mobility of mitochondria [15, 20-22]; however, none of them investigate these interactions in the nervous system of living animals. Though *C. elegans* does not express neurofilaments, several intermediate filaments are expressed in amphids and phasmids sensory neurons of *C. elegans* [6], and specifically IFB-1 has been shown to express in amphid neuron bundles [7]. Importantly, the allele *ju71* carries a deletion in the promoter region of the *ifb-1* gene (Figure 1N) resulting in a reduced expression of IFB-1A (but not IFB-1B) in *C. elegans* as revealed by Western blots [11, 24] and quantitative PCR (Figure 1G). Because *ifb-1* has been reported to be embryonic lethal [7, 8] the remaining expression level of IFB-1B [11, 24] is beneficial, as animals survive (though showing obvious phenotypes such as aberrant epidermis and hook head, Figure 1A) and can be used for experiments. In addition to the *ju71* allele, another allele *ok1317* exists that carries a 1361 bp deletion in the promoter region (upstream of the *ju71* deletion) (Figure 1N). Quantitative PCR revealed that expression of *ifb-1a* is strongly affected in the *ju71* mutant compared to the *ok1317* mutant strain, reflecting also a less obvious phenotype, yet chemotaxis as well as neurite length were significantly reduced (Figure 1D+K+M). We then designed a plasmid that drives the expression of *mito::gfp* (a C-terminal GFP fused to an N-terminal mitochondria-targeting sequence) specifically in amphid neurons using the promoter *Posm-5* [9]. After microinjecting the plasmid, resulting *N2;nthEx4[Posm-5::mito::gfp;rol-6(su1006)]* worms (carrying the roller selection marker pRF4, Figure 1H+I) were then crossed with either CZ4380 *ifb-1(ju71)* or RB1253 *ifb-1(ok1317)* strains, and genotyped to confirm homozygosity. Positioning worms with their vulva sidewise, amphid neurons can be clearly distinguished from labials as amphids seem to adopt the shape of the pharynx and labials are

located closer to the (lateral) cuticle of the worm. Focusing on the amphids with the confocal microscope seems to also exclude labials from imaging as they lie in different focal planes. The somehow shortened and thickened head in the *ju71* background seems to also affect morphologies of amphid neuron bundles which obviously became retracted (Figure 1K); thus we wondered if chemosensation would be affected. To approach this concern, we performed two different assays: Dye filling (Figure 1A+B) as well as chemotaxis quadrant assay (Figure 1C+D). The quantity of dye uptake was comparable between wild type and mutant worms. However, chemotaxis was significantly affected in both mutants, with *ju71* exhibiting the most severe phenotype (Figure 1D) pointing to functional alterations in sensory neurons [42]. Since we observed structural and functional defects in amphid sensory neruons when depleting IFB-1, we wish to understand whether this would imply any physiological consequences of these neurons (for example differences in axonal lengths). For a more straightforward quantification of large quantities of neurons with easily distinguishable polarities (soma, axon and growth cones), we isolated and cultured primary neurons from worm embryos [43]. As a result, we found that dendrite length in worms and neurite length were significantly decreased in cultured neurons (Figure 1K+M). Further, our analysis of life span of mutant worms demonstrated significant reduction in the survival days of both the *ifb-1* mutants (Figure 1E+F).

We then used temporally and spatially high resolution Nipkow spinning disk microscopy to track and analyze the motility of mitochondria in amphid neuron bundles. Single mitochondria can be clearly seen in the amphid bundle (Figure 2E), though the limitation of our microscope did not allow for the discrimination between mitochondria located within distinct neurons in this bundle. For motility assays, we categorized anterograde (Figure 2A) and retrograde (Figure 2B) velocities (without pauses), the occurrences of directional changes (reversals, Figure 2C),

number of pauses in a defined region of the neuron (Figure 2D) (Figure 2E shows a kymograph example of mitochondria motility in wild type and *ju71*). In general, mitochondria motility is comparable between wild type and *ok1317* backgrounds, consistent with our findings of a weak phenotype of this allele (Figure 1). On the other hand, mitochondria mobility was largely affected in the *ju71* background: Speeds were significantly decreased in both directions (Figure 2A and B) with fewer reversals (Figure 2C) and increased resting events (Figure 2D).

Because we found that mitochondria motility is negatively affected when depleting *ifb-1*, we postulate that impeded motility would lead to accumulations and clustering of mitochondria in neurons. Therefore, we analyzed sizes (Figure 3A-C) and densities (Figure 3D) of mitochondria along the dendrites. The first obvious observation was that the area of single mitochondria obviously increased in *ju71* mutants (Figure 3A+B). Consistent with increased areas is also the increase in Feret's diameter (also called "maximum diameter", Figure 3C). More importantly, mitochondria density obviously decreased in both the mutants (Figure 3D), indicating misaccumulation of mitochondria along the dendrites.

The above results indicate that not only mitochondrial mobility is affected when depleting IFB-1, but may also implicate physiological consequences for the neuron, as neurons appear to be shortened (after day 2 in culture). Though future experiments need to evaluate axonal growths at different developmental stages, reduced mobility of mitochondria may affect the metabolic state of neurons leading to shortened axons. On the other hand, mechanical effects might need to be considered, as one of the major functions of the IF cytoskeleton is to stabilize delicate neuronal extensions, and in the case of reduced IF content (IFB-1 depletion) overall elasticity of the neuron may be affected leading to mechanical retractions of axons [44-46]; however assessing these effects is very challenging. Thus, we decided to alter the metabolic state

of mitochondria using the ionophore FCCP (carbonyl cyanide p-(trifluoromethoxy)phenylhydrazone) since this drug is known to discharge the membrane potential of mitochondria that in turn affects their interactions with, e.g., neurofilaments [15]. Because uptake efficiency of FCCP has not been investigated yet, we used cultured neuronal cells to investigate the effect of this ionophore on mitochondria motility. Here, we analyzed complex moving pattern of mitochondria in neurons isolated from wild type worms (expressing *mito::gfp*) with and without 1 μM FCCP (a concentration reported to affect mitochondria-NF interactions, [15]). Interestingly, motility behavior of mitochondria in wild type neurons (Figure 4) is comparable with our motility analysis in live animals (Figure 2). Similarly, in *ju71* mutant backgrounds, motility behavior of mitochondria is comparable with our analysis in live animals (except for "anterograde velocities and directional changes"). More interestingly, the effect of FCCP on mitochondria motility is comparable with the effect of the *ifb-1(ju71)* mutation (Figure 4). The kymograph to the right of Figure 4E shows examples of three different types of mitochondrial motility behaviors in wild type cells (as quantified in left of 4E). Note that DMSO, the solvent for FCCP, did not affect mitochondrial motility. To understand putative effects of *ifb-1(ju71)* mutation on the metabolic state of mitochondria in whole *C. elegans* animals, we employed the XF Extracellular Flux Analyzer (Seahorse Bioscience) that allows for the determination of oxygen consumption from whole animals in solution (though worm's oxygen consumption is linked to complex parameters). Interestingly, the oxygen consumption of whole animals is reduced when carrying the *ifb-1(ju71)* mutation (Figure 5C+D). Further, we also specifically examined amphid sensory neuronal mitochondria for defects in membrane potential using TMRE dye and found that *ifb-1(ju71)* mutants exhibited reduced mitochondrial membrane potential (Figure 5E+F).

Last, we examined colocalization between mitochondria and overexpressed IFB-1A in *C. elegans* amphids. Here, we coinjected a *Posm-5::mito::gfp* construct with a *Posm-5::ifb-1a::mrfp* construct into N2 worms. Figure 6A-D shows the head region of the worm, similar as shown in Figure 1 (H-J). Cell bodies of amphid neurons (located in the nerve ring) are clearly visible to the right from which the dendritic extension of amphid neurons emanate to the tip ("nose") of the worm located to the left (Figure 6A). At this (rather low) magnification distinct IFB-1 particles (or cluster) can be seen in somas (Figure 6B) but barely detected in the dendritic bundles. Thus, we also provide higher magnification images (Figure 6E), revealing single mitochondria (arrows), single IFB-1 aggregates (big arrowhead) or both particles colocalized (small arrow heads). Further, we used images of whole heads of worms (similar to Figure 6C) and determined the intensity correlation quotient (ICQ) revealing significant colocalization events (Figure 6F). Figure 6C is a merged image of Figure 6A and 6B showing various colocalization events in somas; however, to better understand the significance of colocalization, we used the "intensity correlation analysis" plugin from ImageJ (see Methods section). Inspecting the false color scale (more positive values reflect more accurate colocalization) in Figure 6D, significant colocalization is evident in nerve ring cell bodies (arrows). Also, we performed crude mitochondrial pull down to find co-isolated IFB-1::GFP from SW13 (vim-) cells; however, transient expression of only GFP did not co-isolate along with the mitochondrial fraction (Figure 6G).

DISCUSSION

Both mitochondria and neuronal intermediate filaments inherit critical roles in the development of neuropathological incidences [1, 5, 12, 47]. Especially neurons possess high energy demands based on their dedicated functions such as synaptic activities, and consequently mitochondria are of critical importance. Not only dysfunction of mitochondria based on genetic defects or environmental clues (ROS), but also the role of mitochondrial dynamics (fusion and fission events and transport efficiencies) in neurodegeneration has been widely discussed [2, 4, 48-50]. Thus, proper and balanced axonal transport of mitochondria is crucial for neuronal function and viability.

It is well reported how the molecular motors kinesin and dynein power the movement of mitochondria on microtubule tracks, and how myosins move mitochondria on actin tracks; however, mechanisms that lead to the immobilization of mitochondria (specifically at sites of high energy demand) remain to be evaluated. While earlier studies discuss kinase activities (e.g., PI3-kinase, CDK5 or GSK3) that trigger the stops and starts of molecular motors, more recent findings discuss motor receptor molecules (e.g., the miro/milton complex) that regulate the activity of kinesins transporting mitochondria [13, 17, 51]. Alternatively, static anchors such as the microtubule binding protein syntaphilin (SNPH) were demonstrated to actively stop mitochondria at ATP deficient sites [16]. Moreover, it has been shown that neurofilaments (NF) specifically bind to mitochondria and that this interaction depends on the phosphorylation status of the NF side-arms as well on the membrane potential of the mitochondria [15, 32, 52]. Thus, NFs might act as static anchors to immobilize mitochondria at sites of high energy demand, whereas also other types of IFs, e.g., vimentin, have been reported to modulate the dynamics and

organization of mitochondria in fibroblasts [20, 21]. Furthermore, IF-associated proteins such as plectin 1b bear the ability to connect mitochondria to the IF-network in fibroblasts [22].

Because *C. elegans* does not express proteins with similarities to the neurofilament triplet proteins (NF-H, NF-M or NF-L), we searched for other essential IFs which are specifically expressed in neuronal tissues of the nematode. As a result, we found that IFA-1, IFA-2, IFA-3 and IFB-1 are all expressed in neuronal tissues, with IFB-1 revealing the strongest evidence for expression in amphid sensory neurons [7, 8].

C. elegans chemotaxis behavior is largely regulated by the amphid chemosensory organs which are paired bundles of sensory neurons laterally running along the head of the worm (Figure 1H-J). Each amphid bundle contains 11 ciliated chemosensory neurons (and one thermosensory neuron) all sensing a characteristic set of attractants, repellents and pheromones. Somas and (relatively short) axons are both located in the nerve ring from where long dendrites emanate to the tip of the nose where their ciliated endings are exposed to the environment [42, 53]. In most mammalian neurons, microtubule polarity is mixed in dendrites, however, dendrites of *C. elegans* amphid neurons are arranged uniformly, similar to the microtubule arrangement in *D. melanogaster* sensory neurons [54]. Thus, anterograde and retrograde directions of moving mitochondria can be distinguished; though, based on the spatial resolution limitations of our fluorescence microscope, we could not restrict our observation to specific dendrites in the amphid bundle. On the other hand, labial neurons can be easily distinguished from amphid neurons as described in the Method section. This notion is specifically critical as the used promoter *Posm-5* also drives the expression of genes in labials [9, 10] while IFB-1 was not detected in these neurons [7, 8].

The velocities of mitochondria in *C. elegans* neurons (Figure 2 and 4) are comparable with velocities recorded in mammalian systems ranging from 0.32-0.91 μm/s. Similarly, the mobile pool (processive + vibrating mitochondria) was determined to be 50% in *C. elegans* amphid neuron bundles (Figure 4E) which is close to those mobile pools that were determined in mammalian systems (>65%) [3]. The overall effect of IFB-1 suppression on mitochondrial dynamics in our study was a reduced mobility with speed reductions in both anterograde and retrograde directions, consistent with reduced directional changes, increased pausing frequencies in live worms and increased number of stationary mitochondria in neuronal cell cultures (Figure 2 and 4). We may thus speculate that transient interactions with the IF network is critical for stable movements of these large organelles. More importantly, it has been shown that discharged mitochondria lose their ability to connect to neuronal intermediate filaments [15] which is consistent with our observations that the motility behavior of discharged mitochondria after FCCP treatment nearly resembled those in *ifb-1(ju71)* mutant backgrounds (Figure 4).

In our model, the IF network provides additional support and transient anchor points for large mitochondria during their movements on microtubules, and such mechanical support may not be fully provided by the comparably small molecular motors leading to reduced trafficking and misaccumulations. Misaccumulations in turn would likely lead to disturbed metabolism indicated by a decrease in oxygen consumption (Figure 5), developmental defects such as shorter axons (Figure 1K+M) and reduced functions in chemosensations (Figure 1C+D). Importantly, in our model mitochondria interact with the IF network only transiently: during their movement on the microtubule network mitochondria are dynamically attached and detached from IF anchor points. This assumption is in accordance with our colocalization analysis showing that mitochondria are not always in close proximity with IFB-1 cluster (Figure 6E). Our model is also

in accordance with a study that employed NF-L knockout mice showing that the mobile pool of mitochondria increases and mitochondrial movements were more persistent in dorsal root ganglia neurons. Similarly, when these neurons express a mutant type of NF-L (known to cause Charcot-Marie-Tooth disease), the pool of mobile mitochondria was increased, supporting a role of NFs in mitochondrial docking [32, 55]. It is intriguing that IFs might serve as enduring (long-termed) docking sites at localized areas of neurons (with high energy demand) on one hand, but on the other hand to provide only transient (short-termed) attachment points for these large organelles transported by comparably minuscule molecular motors (likely not being able to fully stabilize mitochondria on microtubules). Indeed, it has been suggested that the transport of large vesicular structures along microtubule tracks (in the thin and overcrowded axon, [56]) would find additional support at opposing actin tracks found just below the plasma membrane in axons (actin cortex) [3, 13, 19]. This assumption is consistent with the idea that neuronal IFs (other than NFs) would provide additional mechanical support during the long-range transport of large membranous organelles in long neurites. Our *in vitro* ectopic expression of IFB-1::GFP in SW13 (vim-) cells results in physical interaction between IFB-1 and mitochondrial. Though no protocols exist for the isolation of neuronal mitochondria from *C. elegans*, it might be a legitimate approach to observe the interaction of isolated mitochondria from, e.g., rat brains with *in vitro* polymerized recombinant *C. elegans* IF proteins. Indeed, this study, for the first time, may provide clues for genuine physical interactions between IFB-1 and mitochondria in nematodes (Figure 6). Notably, Leterrier *et al.* 1994 published unique electron micrographs of mitochondria docking to neurofilaments as well as Wagner *et al.* 2003 used atomic force microscopy and TEM to show direct interactions between isolated mitochondria and NFs [15, 57]. Desmin, an abundant IF protein in muscles is linked to various membranous organelles such

as mitochondria, lysosomes, Golgi, etc., and has been implicated to regulate size and shape of mitochondria [58]. Plectin1b encompasses a mitochondrial targeting sequence and lack of plectin1b leads to elongated mitochondria in mouse fibroblast cells [22]. However, IFB-1 does not possess any mitochondrial targeting sequence as predicted by MitoFates (http://mitf.cbrc.jp/MitoFates/cgi-bin/results.cgi?jobId=20190222.111737.13446 . Thus, charged-based weak interactions between IFB-1 and mitochondria may exist. Here, mitochondria with higher membrane potential may interact with negatively charged proteins and indeed the net charge of IFB-1A isoform is -11.6 in the cytoplasm with an isoelectric point of 5.43 (isoelectric.org). In more detail, the head domain of IFB-1A has an isoelectric point of 6.71 and a charge of -0.1 in the cytoplasm, the rod domain inherits an isoelectric point of 5.03 and a charge of -13 in the cytoplasm while the tail domain of IFB-1 has an isoelectric point of 8.35 with a charge of +2.4. Critically, one of our unpublished work demonstrates that TAG-63 is a neurofilament-like protein in *C. elegans*, which can regulate synaptic vesicle's axonal transport possibly utilizing charge based transient interactions.

Having established an observation routine in a widely used model organism that allows for the investigation of mitochondria motility in different IF mutant backgrounds provides a foundation for stimulating future investigations. Though IF proteins are essential, and normally causing severe worm phenotypes, allelic mutant backgrounds exist for the investigation of the effects of other IF types (other than IFB-1) on mitochondrial dynamics [6].

CONCLUSION

We have shown that the depletion of an essential intermediate filament in *C. elegans* causes a reduction in mitochondria mobility with subsequent size and density changes of these organelles in neurons. We relate mitochondrial misaccumulations to a subsequent disturbed metabolism in worms resulting in reduced oxygen consumption and in defects in axonal development. We propose a model in which neuronal intermediate filaments running alongside (and in parallel) with microtubules would stabilize the large and long-shaped mitochondria by providing transient anchor points during their motility. Depletion of this mechanical support would lead to an unbalanced transport of mitochondria. A better understanding of how mitochondrial transport is regulated in neurons may lead to novel insights how various neurological diseases advance providing the basis of future treatments for these emerging diseases.

ACKNOWLEDGEMENTS

We thank the *C. elegans* Core Facility (CECF) Taiwan funded by National Science Council (NSC) for providing us Andrew Fire Vectors, microinjection setups and worm observation systems. We also thank lab members Yu-Fei Peng, Chih-Wei Chen and Víctor Aplícano for their assistance. We also thank Aravind Chandrasekaran for assisting with movie conversions. This work was funded by NSC grants NSC 100-2311-B-007-004 and 101-2311-B-007-002- to OIW.

AUTHORS' CONTRIBUTIONS

YC – Designed as well as performed the experiment and analyzed the data; MMS - Designed as well as performed the experiment, analyzed the data and wrote the manuscript; PB – Performed experiments and analyzed the data; SNB - Performed experiments and analyzed the data; GHW -

Performed experiments and analyzed the data; AFE – Performed experiment; OIW – Designed experiments, obtained grants ad wrote the manuscript.

REFERENCES

1. Perrot, R. and J. Eyer, *Neuronal intermediate filaments and neurodegenerative disorders.* Brain Res Bull, 2009. **80**(4-5): p. 282-95.
2. Cho, D.H., T. Nakamura, and S.A. Lipton, *Mitochondrial dynamics in cell death and neurodegeneration.* Cell Mol Life Sci, 2010. **67**(20): p. 3435-47.
3. Sheng, Z.H. and Q. Cai, *Mitochondrial transport in neurons: impact on synaptic homeostasis and neurodegeneration.* Nat Rev Neurosci, 2012. **13**(2): p. 77-93.
4. Itoh, K., et al., *Mitochondrial dynamics in neurodegeneration.* Trends Cell Biol, 2013. **23**(2): p. 64-71.
5. Millecamps, S. and J.P. Julien, *Axonal transport deficits and neurodegenerative diseases.* Nat Rev Neurosci, 2013. **14**(3): p. 161-76.
6. Carberry, K., et al., *Intermediate filaments in Caenorhabditis elegans.* Cell Motil Cytoskeleton, 2009. **66**(10): p. 852-64.
7. Karabinos, A., et al., *Essential roles for four cytoplasmic intermediate filament proteins in Caenorhabditis elegans development.* Proc Natl Acad Sci U S A, 2001. **98**(14): p. 7863-8.
8. Karabinos, A., et al., *In vivo and in vitro evidence that the four essential intermediate filament (IF) proteins A1, A2, A3 and B1 of the nematode Caenorhabditis elegans form an obligate heteropolymeric IF system.* J Mol Biol, 2003. **333**(2): p. 307-19.
9. Haycraft, C.J., et al., *The C. elegans homolog of the murine cystic kidney disease gene Tg737 functions in a ciliogenic pathway and is disrupted in osm-5 mutant worms.* Development, 2001. **128**(9): p. 1493-505.
10. Simon, J.M. and P.W. Sternberg, *Evidence of a mate-finding cue in the hermaphrodite nematode Caenorhabditis elegans.* Proc Natl Acad Sci U S A, 2002. **99**(3): p. 1598-603.
11. Woo, W.M., et al., *Intermediate filaments are required for C. elegans epidermal elongation.* Dev Biol, 2004. **267**(1): p. 216-29.
12. Martin, L.J., *Mitochondrial pathobiology in Parkinson's disease and amyotrophic lateral sclerosis.* J Alzheimers Dis, 2010. **20 Suppl 2**: p. S335-56.
13. Cai, Q. and Z.H. Sheng, *Mitochondrial transport and docking in axons.* Exp Neurol, 2009. **218**(2): p. 257-67.
14. Morris, R.L. and P.J. Hollenbeck, *Axonal transport of mitochondria along microtubules and F-actin in living vertebrate neurons.* J Cell Biol, 1995. **131**(5): p. 1315-26.
15. Wagner, O.I., et al., *Mechanisms of mitochondria-neurofilament interactions.* J Neurosci, 2003. **23**(27): p. 9046-58.
16. Kang, J.S., et al., *Docking of axonal mitochondria by syntaphilin controls their mobility and affects short-term facilitation.* Cell, 2008. **132**(1): p. 137-48.
17. Hollenbeck, P.J. and W.M. Saxton, *The axonal transport of mitochondria.* J. Cell Sci., 2005. **118**: p. 5411-5419.
18. Hirokawa, N., S. Niwa, and Y. Tanaka, *Molecular motors in neurons: transport mechanisms and roles in brain function, development, and disease.* Neuron, 2010. **68**(4): p. 610-38.
19. Boldogh, I.R. and L.A. Pon, *Mitochondria on the move.* Trends Cell Biol, 2007. **17**(10): p. 502-10.

20. Nekrasova, O.E., et al., *Vimentin intermediate filaments modulate the motility of mitochondria.* Mol Biol Cell, 2011. **22**(13): p. 2282-9.
21. Tang, H.L., et al., *Vimentin supports mitochondrial morphology and organization.* Biochem J, 2008. **410**(1): p. 141-6.
22. Winter, L., C. Abrahamsberg, and G. Wiche, *Plectin isoform 1b mediates mitochondrion-intermediate filament network linkage and controls organelle shape.* J Cell Biol, 2008. **181**(6): p. 903-11.
23. Brenner, S., *The genetics of Caenorhabditis elegans.* Genetics, 1974. **77**(1): p. 71-94.
24. Kaminsky, R., et al., *SUMO regulates the assembly and function of a cytoplasmic intermediate filament protein in C. elegans.* Dev Cell, 2009. **17**(5): p. 724-35.
25. Bae, Y.K., et al., *Identification of genes involved in the ciliary trafficking of C. elegans PKD-2.* Dev Dyn, 2008. **237**(8): p. 2021-9.
26. Fire, A., *Integrative transformation of Caenorhabditis elegans.* Embo J, 1986. **5**(10): p. 2673-2680.
27. Mello, C.C., et al., *Efficient gene transfer in C.elegans: extrachromosomal maintenance and integration of transforming sequences.* EMBO J, 1991. **10**(12): p. 3959-70.
28. Wagner, O.I., et al., *Synaptic scaffolding protein SYD-2 clusters and activates kinesin-3 UNC-104 in C. elegans.* Proc Natl Acad Sci U S A, 2009. **106**(46): p. 19605-10.
29. Tong, Y.G. and T.R. Burglin, *Conditions for dye-filling of sensory neurons in Caenorhabditis elegans.* J Neurosci Methods, 2010. **188**(1): p. 58-61.
30. Margie, O., C. Palmer, and I. Chin-Sang, *C. elegans chemotaxis assay.* J Vis Exp, 2013(74): p. e50069.
31. Kocsis, E., et al., *Image averaging of flexible fibrous macromolecules: the clathrin triskelion has an elastic proximal segment.* J Struct Biol, 1991. **107**(1): p. 6-14.
32. Gentil, B.J., et al., *Normal role of the low-molecular-weight neurofilament protein in mitochondrial dynamics and disruption in Charcot-Marie-Tooth disease.* FASEB J, 2012. **26**(3): p. 1194-203.
33. Li, Q., et al., *A syntaxin 1, Galpha(o), and N-type calcium channel complex at a presynaptic nerve terminal: analysis by quantitative immunocolocalization.* J Neurosci, 2004. **24**(16): p. 4070-81.
34. Mondal, S., et al., *Imaging in vivo neuronal transport in genetic model organisms using microfluidic devices.* Traffic, 2011. **12**(4): p. 372-85.
35. Hoogewijs, D., et al., *Selection and validation of a set of reliable reference genes for quantitative sod gene expression analysis in C. elegans.* BMC Mol Biol, 2008. **9**: p. 9.
36. Yamamoto, H., et al., *NCoR1 is a conserved physiological modulator of muscle mass and oxidative function.* Cell, 2011. **147**(4): p. 827-39.
37. Sutphin, G.L. and M. Kaeberlein, *Measuring Caenorhabditis elegans life span on solid media.* J Vis Exp, 2009(27).
38. Park, H.H., Y. Jung, and S.V. Lee, *Survival assays using Caenorhabditis elegans.* Mol Cells, 2017. **40**(2): p. 90-99.
39. Michael Christensen, et al., *A Primary culture system for functional analysis of C. elegans neurons and muscle cells.* Neuron, 2002. **33**: p. 503-514.
40. Kevin Strange, Michael Christensen, and R. Morrison, *Primary culture of Caenorhabditis elegans developing embryo cells for electrophysiological, cell biological and molecular studies.* Nature Protocols, 2007. **2**: p. 1003-1012.
41. Sarasija. S and N. K.R., *Analysis of mitochondrial structure in the body wall muscle of Caenorhabditis elegans. .* Bio-protocol, 2018. **8**(7): p. e2801.
42. Bargmann, C.I. and I. Mori, *Chemotaxis and Thermotaxis*, in *C. elegans II*, D.L. Riddle, et al., Editors. 1997: Cold Spring Harbor (NY).

43. Strange, K., M. Christensen, and R. Morrison, *Primary culture of Caenorhabditis elegans developing embryo cells for electrophysiological, cell biological and molecular studies.* Nat Protoc, 2007. **2**(4): p. 1003-12.
44. Franze, K., *The mechanical control of nervous system development.* Development, 2013. **140**(15): p. 3069-77.
45. Tang-Schomer, M.D., et al., *Mechanical breaking of microtubules in axons during dynamic stretch injury underlies delayed elasticity, microtubule disassembly, and axon degeneration.* FASEB J, 2010. **24**(5): p. 1401-10.
46. Lele, T.P. and S. Kumar, *Brushes, cables, and anchors: recent insights into multiscale assembly and mechanics of cellular structural networks.* Cell Biochem Biophys, 2007. **47**(3): p. 348-60.
47. Ankarcrona, M., F. Mangialasche, and B. Winblad, *Rethinking Alzheimer's disease therapy: are mitochondria the key?* J Alzheimers Dis, 2010. **20 Suppl 2**: p. S579-90.
48. Knott, A.B., et al., *Mitochondrial fragmentation in neurodegeneration.* Nat Rev Neurosci, 2008. **9**(7): p. 505-18.
49. Su, B., et al., *Abnormal mitochondrial dynamics and neurodegenerative diseases.* Biochim Biophys Acta, 2010. **1802**(1): p. 135-42.
50. Chen, H. and D.C. Chan, *Mitochondrial dynamics — fusion, fission, movement, and mitophagy — in neurodegenerative diseases.* Hum. Mol. Genet., 2009. **18**: p. 169-176.
51. Saxton, W.M. and P.J. Hollenbeck, *The axonal transport of mitochondria.* J Cell Sci, 2012. **125**(Pt 9): p. 2095-104.
52. Leterrier, J.F., et al., *Interactions between brain mitochondria and cytoskeleton: evidence for specialized outer membrane domains involved in the association of cytoskeleton-associated proteins to mitochondria in situ and in vitro.* Microsc Res Tech, 1994. **27**(3): p. 233-61.
53. Bargmann, C.I., *Chemosensation in C. elegans.* WormBook, 2006: p. 1-29.
54. Maniar, T.A., et al., *UNC-33 (CRMP) and ankyrin organize microtubules and localize kinesin to polarize axon-dendrite sorting.* Nat Neurosci, 2012. **15**(1): p. 48-56.
55. Perrot, R. and J.P. Julien, *Real-time imaging reveals defects of fast axonal transport induced by disorganization of intermediate filaments.* FASEB J, 2009. **23**(9): p. 3213-25.
56. Hirokawa, N., *Cross-linker system between neurofilaments, microtubules, and membranous organelles in frog axons revealed by the quick-freeze, deep-etching method.* J. Cell Biol., 1982. **94**: p. 129-142.
57. Leterrier, J.F., et al., *Interactions between brain mitochondria and cytoskeleton: Evidence for specialized outer membrane domains involved in the association of cytoskeleton-associated proteins to mitochondria in situ and in vitro.* Microscopy Research Technique, 1994. **27**(3).
58. Capetanaki, Y., et al., *Muscle intermediate filaments and their links to membranes and membranous organelles.* Exp Cell Res, 2007. **313**(10): p. 2063-76.

FIGURE LEGENDS

Figure 1: Characterization of *ifb-1* mutants. (A) Representative images of ciliated endings of amphid dendrites at the nose of various worms (N2 control, *ok1317* and *ju71* mutants) after dye-filling. Arrow indicates structural deformaties in *ju71* mutant (hook-head phenotype). (B) Dye-filling quantification (N = 300 worms). (C) Pictorial presentative (left panel) and photograph of representative plates (right panel) of quadrant chemotaxis assay. (D) Determined chemotaxis index in different genetic backgrounds (N = 30-150 worms with 9 trials). (E) Percentage survival rate (N = 40-59 worms) and (F) Average survival days of worms from different genetic backgrounds. (G) Quantitative PCR analysis of *ifb-1* mRNA expression. (H) Confocal z-stack images of N2 worms expressing *Posm-5::mito::gfp* superimposed with maximum intensity. Dashed outline represents the margins of the worm's head. (I) Mitochondria in amphids from dashed rectangle in (H). (J) *ifb-1(ju71)* mutant expressing *Posm-5::mito::gfp*. (K) Quantification of dendrite length from somas of amphid neurons (located in the nerve ring) to the region of the dendrite where cilia begin to emanate (to the nose), N = 12-13 worms. (L) Representative images of cultured worm neurons from different genetic background. (M) Quantification of axonal length from (L), N = 10 cells. (N) Graphical representation of ifb-1 exon/intron gene structure and the revealed location of the deletion mutations. Scale bars: 10 µm in (A) as well as (H-J and L) and 1 mm in (C). Error bars: ± max. and min. range. One-way ANOVA with Fisher's LSD test (D, F, G), Student's t-test (K) and Gehan-Breslow-Wilcoxon test (E). * $p<0.05$, ** $p<0.01$, *** $p<0.001$ and **** $p<0.0001$. A – anterior direction and P – posterior direction.

Figure 2: **Motility analysis of mitochondria in amphid neuron bundles of living *C. elegans*.** Compared to wt (referred to strain *N2;nthEx4[Posm-5::mito::gfp;rol-6(su1006)]*), the velocity significantly decreased in both (A) anterograde and (B) retrograde directions in *ju71* allelic

backgrounds (strain *ifb-1(ju71);nthEx4[Posm-5::mito::gfp;rol-6(su1006)]*. Parameters in the *ifb-1(ok1317)* mutant background (strain *ifb-1(ok1317);nthEx4[Posm-5::mito::gfp;rol-6(su1006)]*)) largely resemble wt phenotypes. (C) Quantification of directional changes in different genetic background. (D) Similarly, because speeds are reduced in *ju71* mutants, pause frequency increased in these mutants. (E) Representative kymographs of mitochondria movements in wild type and *ju71*. Total number of analyzed moving events: 1210 for wt, 742 for *ifb-1(ju71)* and 1201 for *ok1317*. One-way ANOVA with Fisher's LSD test: *p>0.1, **p>0.05. Error bars: ± SEM. Horizontal scale bar: 10 µm. Vertical scale bar: 20 s.

Figure 3: **Mitochondrial accumulation in *ifb-1* mutants.** (A) Straightened and stacked amphid dendrites from different genetic backgrounds. (B) Quantification of mitochondrial size in these dendrites (wild type and *ifb-1* mutants). (C) Quantification of Feret's diameter from images in (A). (D) Density quantification of mitochondria in wild type and *ifb-1* mutants. Scale bar: 10 µm. Error bars: ± max. and min. range. N = 559-841 particles in (B+C), N = 15-17 dendrites in (D). One-way ANOVA with Fisher's LSD test. * p<0.05 and ****p<0.0001.

Figure 4: **Motility analysis comparison between FCCP (1 µM) treated N2 and *ju71* mitochondria.** Quantification of anterograde velocity (A), retrograde velocity (B), directional changes (C), pausing duration (D). (E) Kymograph revealing vibrating (1), processive (2) and stationary (3) mitochondria (left panel) and percentage of mitochondria in different motility state (right panel). Total number of analyzed moving events: 3697 for wt and 2217 for *ifb-1(ju71).* Horizontal scale bar: 10 µm. Vertical scale bar: 20 s. Error bars: ± SEM. One-way ANOVA with Fisher's LSD test. *p<0.05.

Figure 5: **Physiologically defective mitochondria in *ifb-1(ju71)* mutants.** (A) Oxygen consumption in N2 control and *ifb-1(ok1317)* mutants. (B) Oxygen consumption over the assay period of 120 min. (C) Oxygen consumption in N2 control and *ifb-1(ju71)* worms. (D) Oxygen consumption over the assay period. (E) Representative worm images *expressing Posm-5::mito::gfp* stained with TMRE dye in different genetic background. (F) ICQ quantification of MITO::GFP and TMRE staining in different genetic background, N = 13 to 17 worms. Error bars: ± max. and min. range. N = 50 worms per well with 10 wells/study group in a 24 wells plate (A-D). Student's t-test. *p<0.05, **p<0.01.

Figure 6: **Mitochondria/IFB-1 colocalization and pull downs.** (A-D) Images of wild type worms expressing MITO::GFP as well as IFB-1::mRFP (both under the Posm-5 promoter). A – anterior direction and P – posterior direction. (E) Stacks of straightened dendrites digitally magnified. Short arrow points to colocalization, arrow heads point to IFB-1 particles, long arrow points to single mitochondrion. (F) ICQ quantification of IFB-1/mitochondria colocalization from (C). (G) Western blot of crude mitochondrial fraction (Mito) and cytosolic fraction (Cyto) isolated from SW13 (vim-) cells expressing either IFB-1::GFP (left panel) or only GFP (right panel). Scale bars: 20 µm in (A-D) and 5 µm in (E). Error bars: ± max. and min. range. N = 28 worms.

Figure 7: **IFs physically support mitochondrion during their long-range transport.** Pictorial representation of additional mechanical support provided by IFs for the transport of (comparatively) large mitochondrion by (comparatively) miniature kinesins. Dynein motors not shown. Transient interactions between the mitochondrion and IFB-1 along neurites might support motors on MT tracks for more efficient transport.

Supplemental Video 1: Video sequence of recorded mitochondria movements in amphid sensory neurons of (A) wt and (B) *ju71* (same animals as described in Figure 2). Time-lapse factor: 4x (28 frames per second). Mobility of mitochondria in *ju71* animal is obviously reduced.

FIGURES

Figure 1

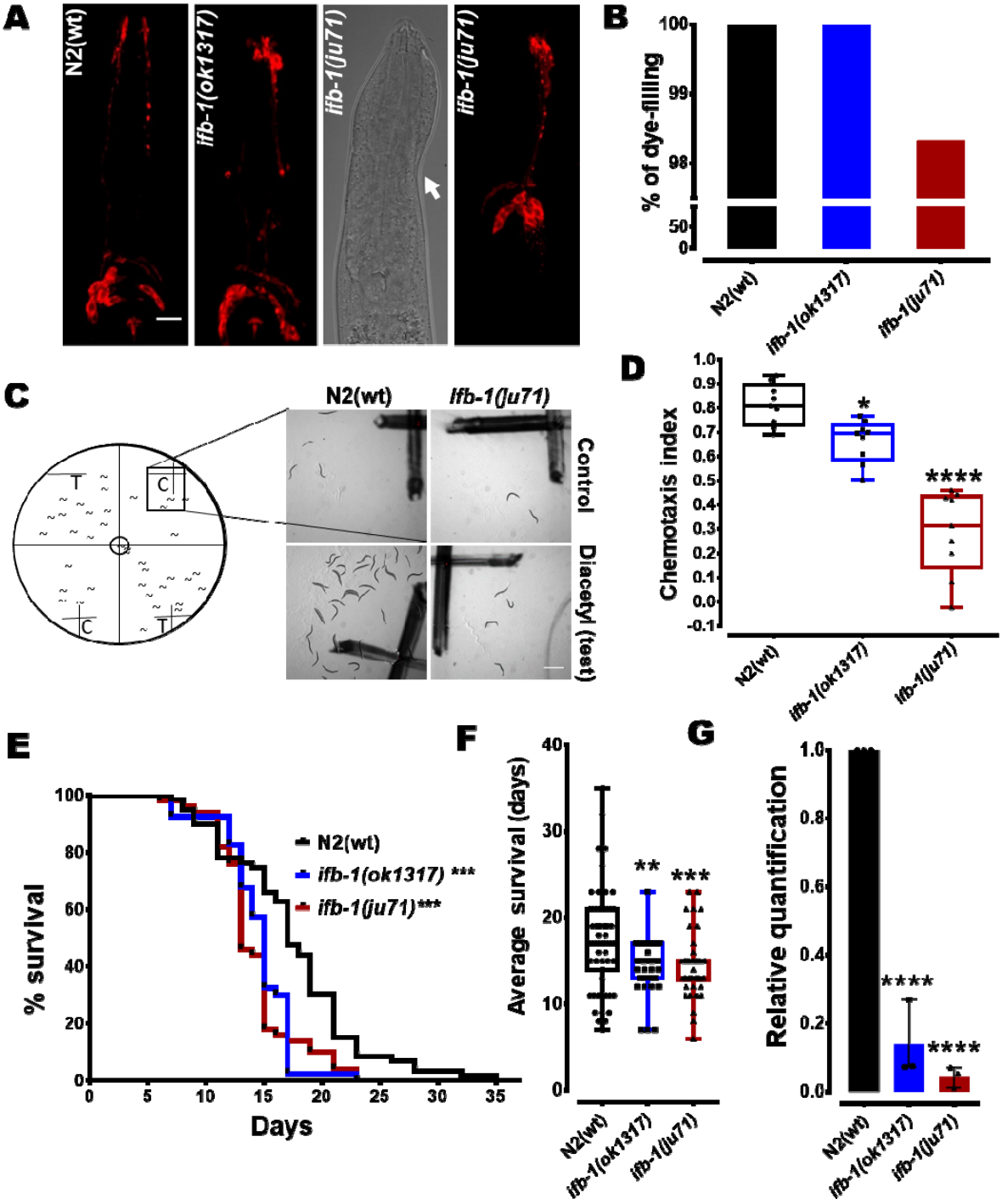

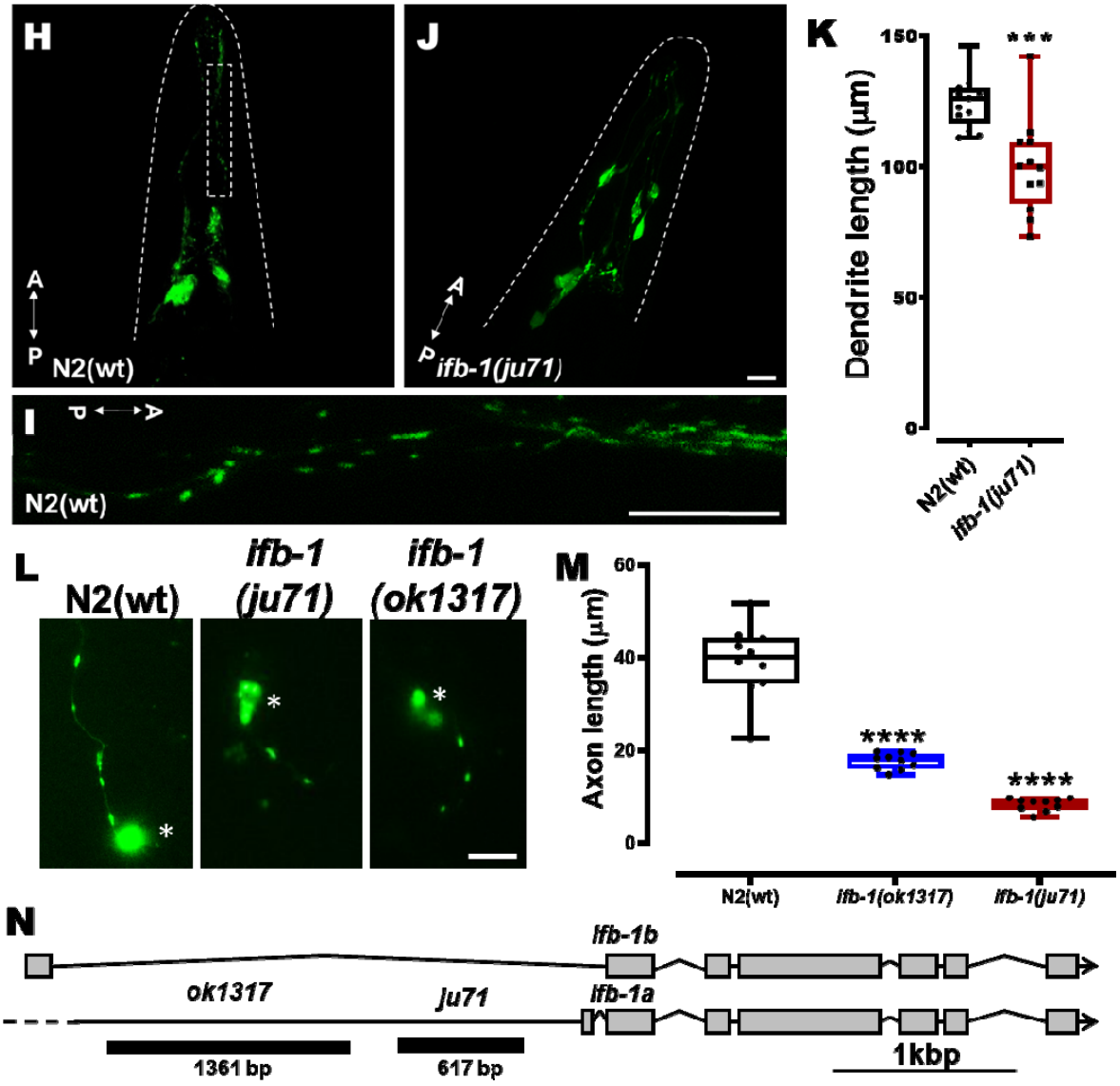
H
A
P
N2(wt)
J
A
P
ifb-1(ju71)
I
P
A
N2(wt)
K
Dendrite length (μm)
150
100
50
0
***
N2(wt)
ifb-1(ju71)
L
N2(wt)
ifb-1 (ju71)
ifb-1 (ok1317)
M
Axon length (μm)
60
40
20
0
****
****
N2(wt)
ifb-1(ok1317)
ifb-1(ju71)
N
ifb-1b
ok1317
ju71
ifb-1a
1361 bp
617 bp
1kbp

Figure 2

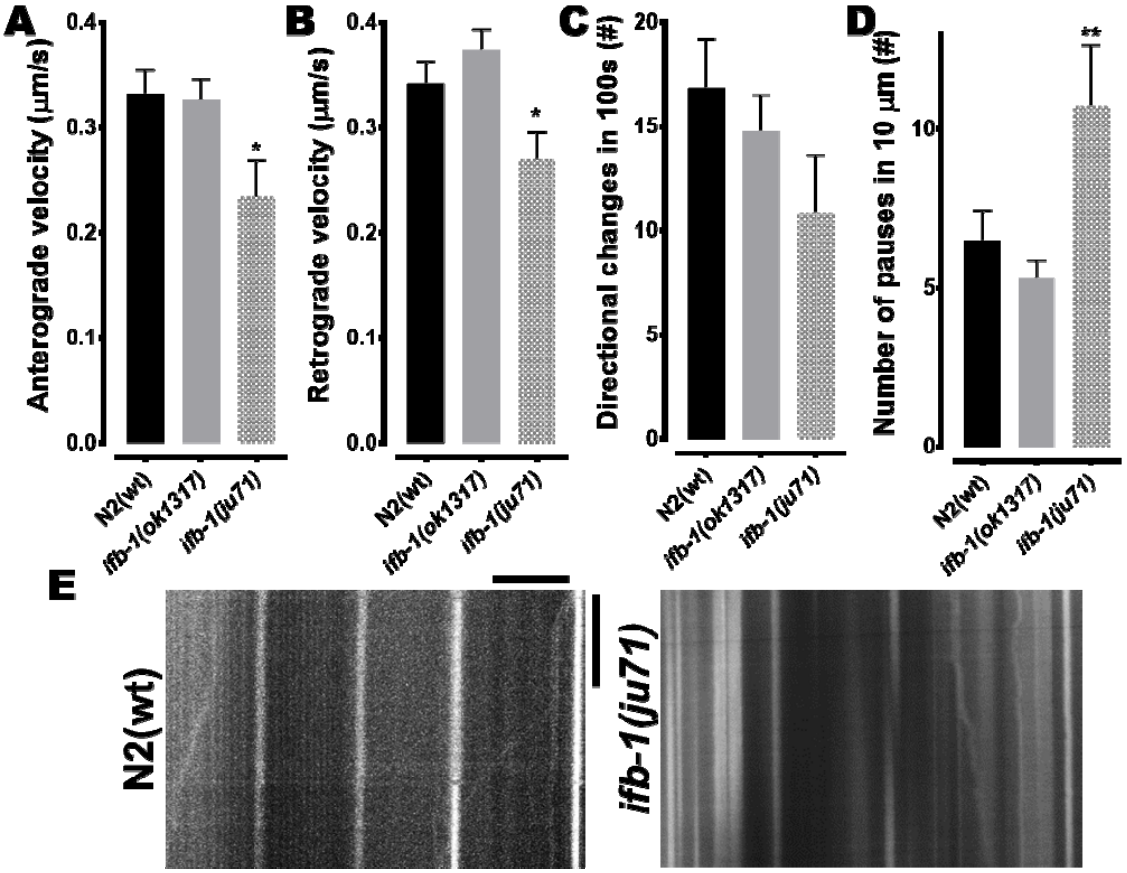
A
Anterograde velocity (μm/s)
0.4
0.3
0.2
0.1
0.0
*
N2(wt)
ifb-1(ok1317)
ifb-1(ju71)
B
Retrograde velocity (μm/s)
0.4
0.3
0.2
0.1
0.0
*
N2(wt)
ifb-1(ok1317)
ifb-1(ju71)
C
Directional changes in 100s (#)
20
15
10
5
0
N2(wt)
ifb-1(ok1317)
ifb-1(ju71)
D
Number of pauses in 10 μm (#)
10
5
0
**
N2(wt)
ifb-1(ok1317)
ifb-1(ju71)
E
N2(wt)
ifb-1(ju71)

Figure 3

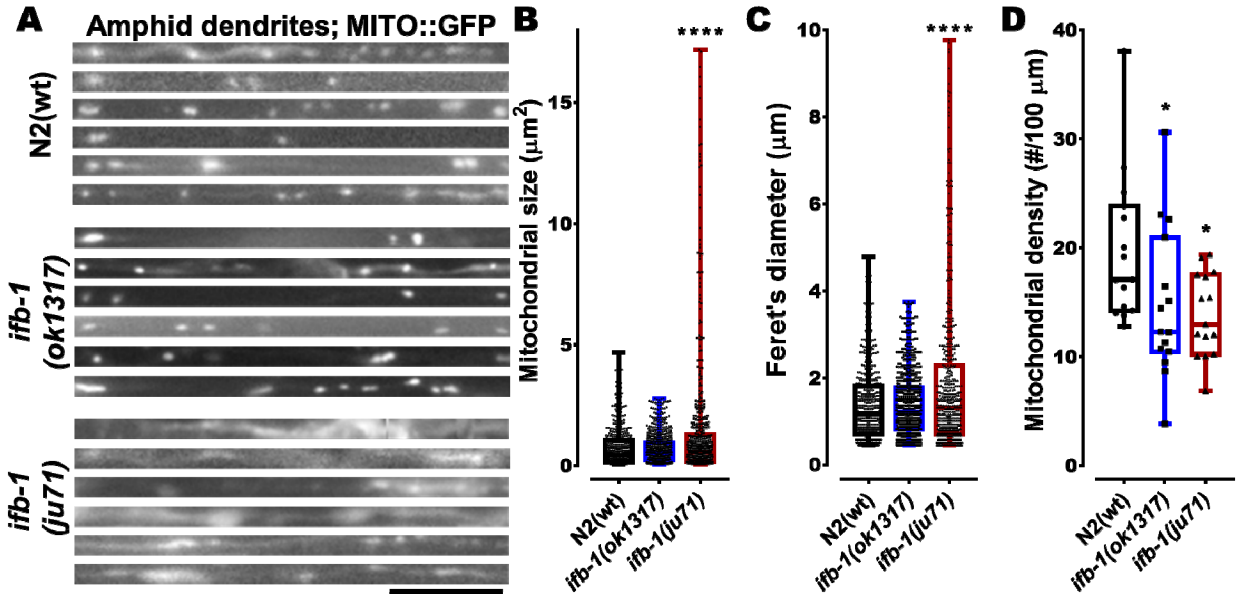
A
Amphid dendrites; MITO::GFP
N2(wt)
ifb-1 (ok1317)
ifb-1 (ju71)
B
Mitochondrial size (μm²)
****
C
Feret's diameter (μm)
****
D
Mitochondrial density (#/100 μm)
*
*
N2(wt)
ifb-1(ok1317)
ifb-1(ju71)

Figure 4

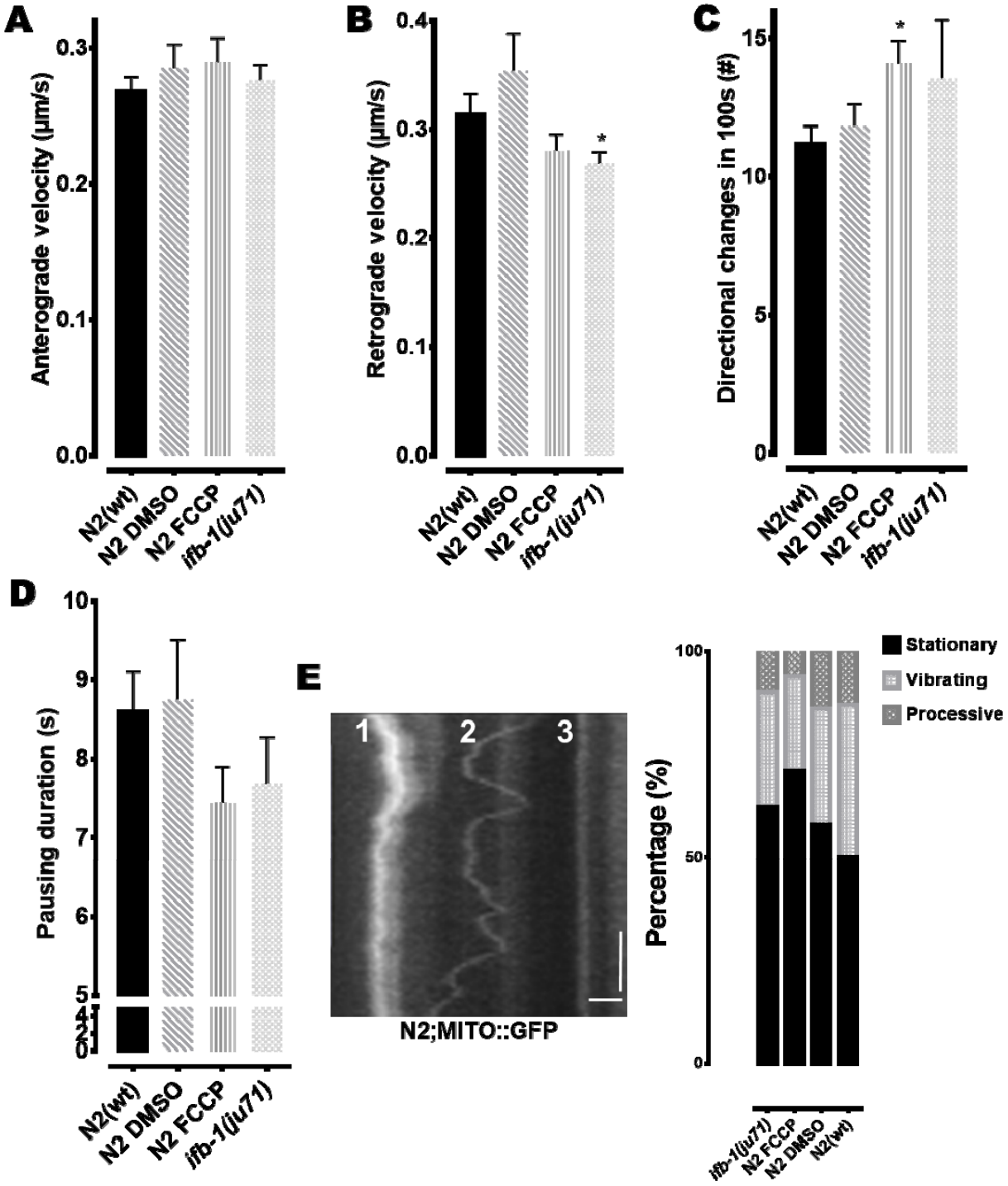
A
Anterograde velocity (µm/s)
0.0
0.1
0.2
0.3
N2(wt)
N2 DMSO
N2 FCCP
ifb-1(ju71)
B
Retrograde velocity (µm/s)
0.0
0.1
0.2
0.3
0.4
*
C
Directional changes in 100s (#)
0
5
10
15
*
D
Pausing duration (s)
5
6
7
8
9
10
E
1
2
3
N2;MITO::GFP
Percentage (%)
0
50
100
Stationary
Vibrating
Processive

Figure 5

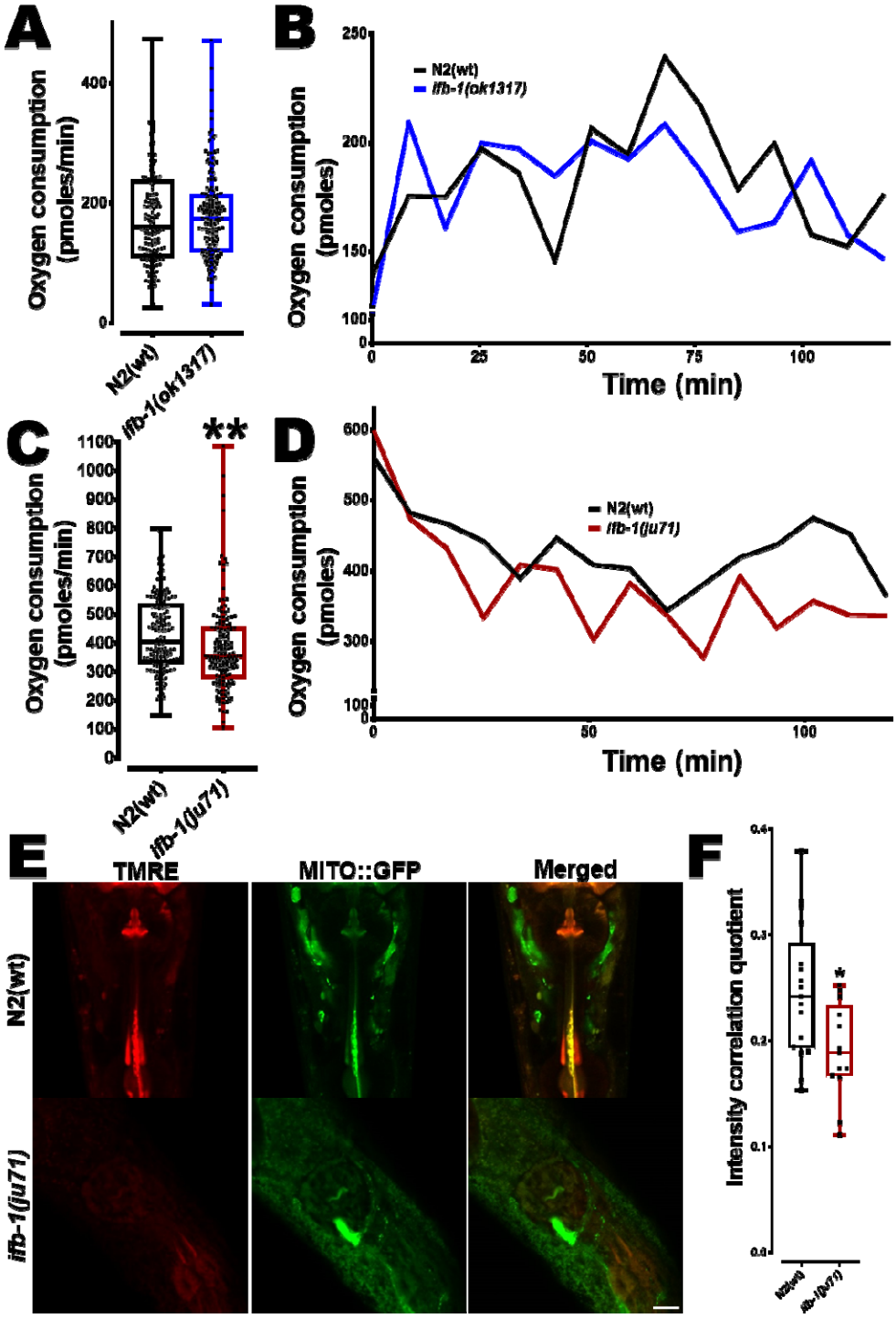
A
Oxygen consumption (pmoles/min)
N2(wt)
ifb-1(ok1317)
B
Oxygen consumption (pmoles)
N2(wt)
ifb-1(ok1317)
Time (min)
C
Oxygen consumption (pmoles/min)
**
N2(wt)
ifb-1(ju71)
D
Oxygen consumption (pmoles)
N2(wt)
ifb-1(ju71)
Time (min)
E
TMRE
MITO::GFP
Merged
N2(wt)
ifb-1(ju71)
F
Intensity correlation quotient
*
N2(wt)
ifb-1(ju71)

Figure 6

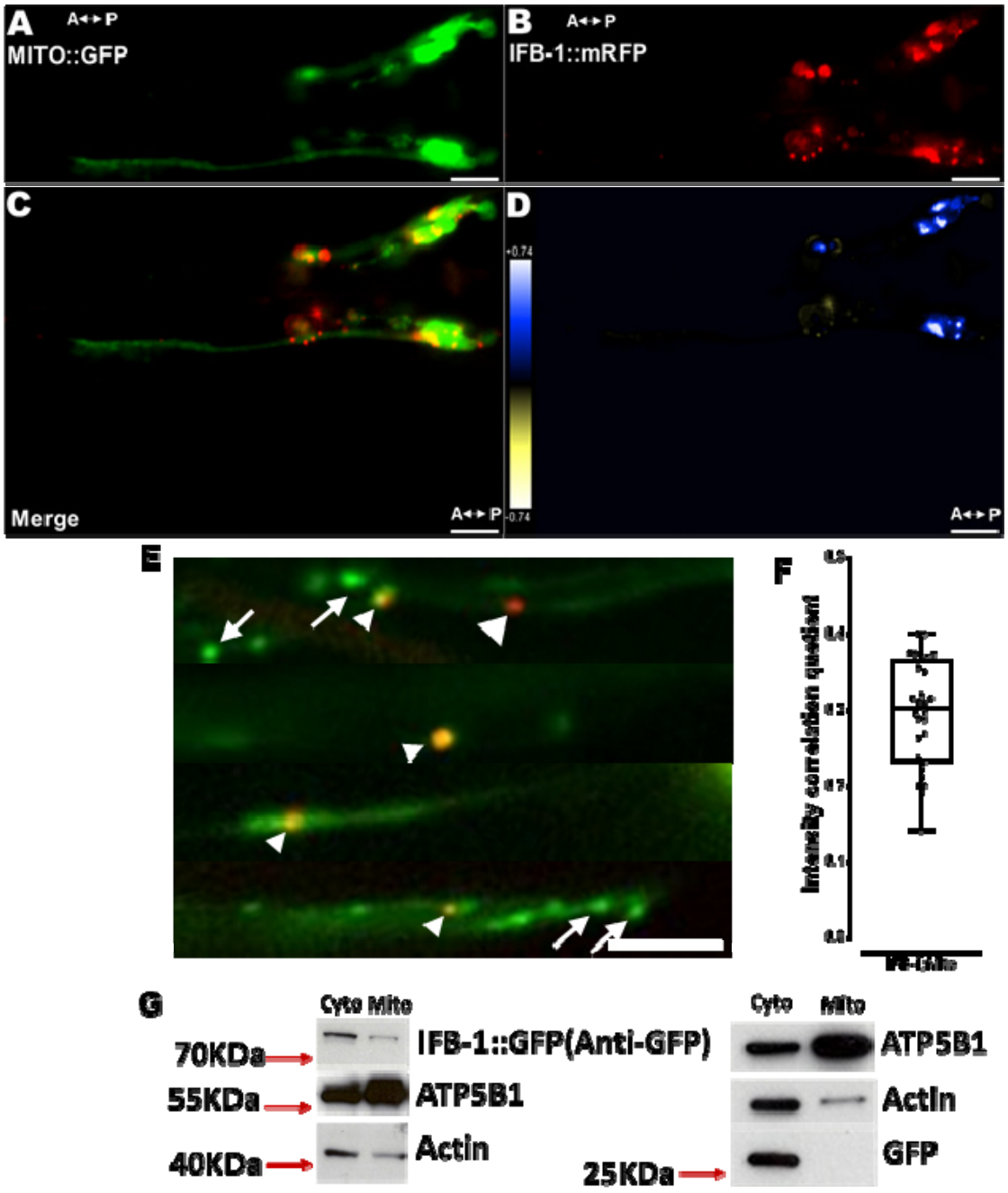
A
A↔P
MITO::GFP
B
A↔P
IFB-1::mRFP
C
Merge
A↔P
D
+0.74
-0.74
A↔P
E
F
Intensity correlation quotient
G
Cyto Mito
70KDa
IFB-1::GFP(Anti-GFP)
55KDa
ATP5B1
40KDa
Actin
Cyto
Mito
ATP5B1
Actin
25KDa
GFP
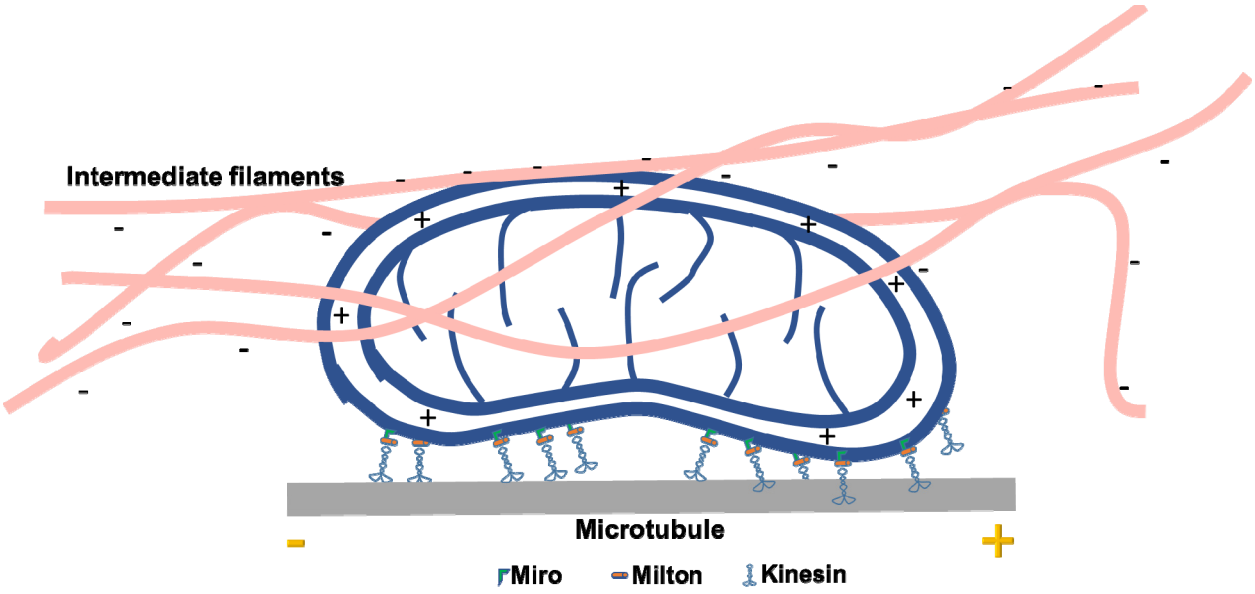
Figure 7